Physical and stoichiometric controls on stream respiration in a headwater stream

Jancoba Dorley[1], Joel Singley[2,3], Tim Covino[4,5], Kamini Singha[6], Michael Gooseff[7,8], David Van Horn[9], Ricardo González-Pinzón[1]

Correspondence to: Ricardo González-Pinzón (gonzaric@unm.edu)

[1]Civil, Construction and Environmental Engineering, University of New Mexico, Albuquerque, NM USA
[2]Environmental Studies Program, University of Colorado, Boulder, CO USA
[3]Biology, Marine Biology, and Environmental Science, Roger Williams University, Bristol, RI USA
[4]Ecosystem Science and Sustainability, Colorado State University, Fort Collins, CO USA
[5]Department of Land Resources and Environmental Sciences, Montana State University, Bozeman, MT USA
[6]Geology and Geological Engineering, Hydrologic Science and Engineering Program, Colorado School of Mines, Golden, CO USA
[7]Civil, Environmental and Architectural Engineering, University of Colorado, Boulder, CO USA
[8]Institute of Arctic and Alpine Research, University of Colorado, Boulder, CO USA
[9]Department of Biology, University of New Mexico, Albuquerque, NM USA

Abstract. Many studies in ecohydrology focusing on hydrologic transport argue that longer residence times across a stream ecosystem should consistently result in higher biological uptake of carbon, nutrients, and oxygen. This consideration does not incorporate the potential for biologically mediated reactions to be limited by stoichiometric imbalances. Based on the relevance and co-dependences between hydrologic exchange, stoichiometry, and biological uptake, and acknowledging the limited amount of field studies available to determine their net effects on the retention and export of resources, we quantified how microbial respiration is controlled by the interactions and supply of essential nutrients (C, N, P) in a headwater stream in Colorado, USA. For this, we conducted two rounds of nutrient experiments, each consisting of four sets of continuous injections of Cl- as a conservative tracer, resazurin as a proxy for aerobic respiration, and one of the following nutrient treatments: a) N, b) N+C, c) N+P, and d) C+N+P. Nutrient treatments were considered as known system modifications to alter metabolism, and statistical tests helped identify the relationships between hydrologic transport and respiration metrics. We found that as discharge changed significantly between rounds and across stoichiometric treatments, a) transient storage mainly occurred in pools lateral to the main channel and was proportional to discharge, and b) microbial respiration remained similar between rounds and across stoichiometric treatments. Our results contradict the notion that hydrologic transport alone is a dominant control on biogeochemical processing and suggest that complex interactions between hydrology, resource supply, and biological community function are responsible for driving in-stream respiration.

1 Introduction

High biochemical processing rates in streams and rivers occur at locations and times where the dynamic interconnections among hydrologic exchange, residence time, nutrient supply, and microbial biomass combine to form optimum conditions for metabolic activity (i.e., the transformation of nutrients, carbon, and oxygen or another electron acceptor into energy and biomass). The exchange of water between the main channel and transient storage zones, where most microbes exist, is the primary mechanism supplying carbon, nutrients, and oxygen to metabolically active zones (Gooseff et al. 2004; Covino et al. 2010b, 2011; Knapp et al. 2017; Gootman et al. 2020). The extent of water exchange controls the residence time of solutes (Drummond et al., 2012; Gomez et al., 2012; Patil et al., 2013), their chemical signatures (Covino and McGlynn 2007), as well as the microbial composition and their metabolic functioning (Blume et al. 2002; Navel et al. 2011; Li et al. 2020). Exchange patterns are influenced by geomorphologic conditions (Kasahara and Wondzell 2003; Cardenas et al. 2004; Gooseff et al. 2005; Emanuelson et al. 2022), hydrologic conditions (i.e., discharge and surrounding water table configuration) (Gooseff et al. 2005; Wondzell 2006; Ward et al. 2013; Ward and Packman 2019), and biofilm growth (Battin et al. 2003; Wen and Li 2018). The spatiotemporal variability in exchange processes and resource availability (e.g., seasonal variations in nutrient loads) create heterogeneous hydrologic and biogeochemical gradients across space and time, within which ecosystem metabolism occurs (Mulholland et al., 1985; Mulholland & Hill, 1997).

To date, studies with a focus on hydrologic transport argue that longer residence times across a stream ecosystem should consistently result in higher biological demand for carbon, nutrients, and oxygen (Valett et al. 1996; Gooseff et al. 2005; Wondzell 2006; Gomez et al. 2012; Zarnetske et al. 2012; Ward et al. 2013; Li et al. 2021), not fully incorporating the potential for biologically mediated reactions to be limited by stoichiometric imbalances. Ecological stoichiometry is the notion that biota balance the consumption of nutrients with energy requirements. Redfield (1934) noted that marine phytoplankton generally contained a ratio of C:N:P of 106:16:1 in their biomass, and these ratios are similar to those available in their environment. This "Redfield ratio" suggests that an ecosystem requires an optimal ratio of available nutrients to flourish and has been used as a guide for many other environmental stoichiometry studies. In a study of streams across eight biomes, Dodds et al. (2004) noted that N consumption depends in part on the C:N ratio of organic matter in streams and suggested that shifts in these state ratios likely influence N retention.

The net effect of supply and demand of resources can be explored with the non-dimensional Damköhler number, Da (Harvey et al. 2013; Pinay et al. 2015; Krause et al. 2017; Ocampo et al. 2020), which quantifies the ratio of transport (i.e., supply) to biological uptake (i.e., demand) timescales along flow paths (Oldham et al. 2013; Liu et al. 2022). Similar to any other non-dimensional number, Da offers simplicity and objectivity for inter-site and intra-site comparisons. Da has been used to provide insight into the factors limiting the supply and demand of resources (Harvey et al. 2005), as values of $Da \sim 1$ define a balance between transport and uptake time scales, which theoretically result in maximal resource retention. Accordingly, where or when $Da \ll 1$, i.e., the uptake timescale is much greater than the transport timescale, uptake is suboptimal, and it is referred to as reaction limited because even though resources became available through hydrologic exchange, they were not fully taken up (i.e., assimilated).

73 Conversely, where or when *Da* >>1, i.e., the transport timescale is much greater than the uptake timescale, resources

74 become scarce or transport-limited, and biologically inactive subregions start to develop (González-Pinzón and

75 Haggerty 2013; Harvey et al. 2013; Gootman et al. 2020). While *Da* captures essential components of the potential

76 interactions between the supply and demand of ecologically relevant resources, it does not explicitly capture the role

77 of stoichiometric limitations on the supply (i.e., C:N:P ratios in water fluxes) and demand (C:N:P biomass

78 composition and needs) of resources (Tromboni et al. 2018). This is because *Da* numbers are estimated from solute-

79 specific mass balances, which inform transport and reaction timescales for one resource at a time (e.g., only N), in

80 isolation of other stoichiometrically relevant resources that can become limiting factors (e.g., C and P).

81 Based on the relevance and co-dependences between hydrologic exchange, stoichiometry, and biological

82 uptake, and the limited amount of field studies available to determine their net effects on the retention and export of

83 resources, we sought to quantify how metabolic activity is controlled by the interactions and supply of essential

84 nutrients (C, N, P). More specifically, we tested if variations in stoichiometric conditions can induce metabolic

85 limitations at which residence time alone becomes a weak predictor of stream respiration. We addressed the

86 following research question: *How is microbial respiration controlled by hydrologic exchange vs. stoichiometric*

87 *conditions (i.e., supply of C, N, and P)*? We hypothesized that aerobic respiration would be maximized when

88 nutrient supply and demand were nearly balanced for a given hydrologic condition. To test this, we conducted a

89 repeated set of stream tracer injections in Como Creek, a mountain stream in Colorado, USA, varying stream C

90 (acetate; sensu Baker et al., 1999), N ($NaNO_3$), and P (KH_2PO_4) concentrations to manipulate stoichiometry and

91 nutrient supply. We repeated experiments under different flow conditions to quantify the tradeoffs between supply

92 (transport and delivery of nutrients), and demand (microbial respiration). We tested for statistical relationships

93 between hydrologic transport metrics and respiration metrics using the resazurin-resorufin tracer system (González-

94 Pinzón et al., 2012; Knapp et al., 2018) and contextualized our findings within the framework of the Damköhler

95 number.

96 **2 Methods**

97 **2.1 Site Description**

98 Our research experiments were conducted in Como Creek, a forested pool and riffle stream in Colorado,

99 USA. Como Creek is a tributary to Boulder Creek, with land cover consisting of approximately 20% alpine

100 meadow-tundra and 80% conifer forest. The study reach drains a 5.4 km^2 catchment, with elevations ranging from

101 2895-3557 m and a mean average precipitation of 883 mm/y (Ries III et al. 2017; Emanuelson et al. 2022). Como

102 Creek has a snowmelt-driven hydrograph with stream discharges ranging from 1-98 L/s and features short-lived

103 increases in discharge during the monsoon season between July and August (Figure 1). The study reach is a multi-

104 thread channel with substrate ranging from small gravel to bedrock. Additionally, the channel has an average width-

105 to-depth ratio of 11.5, a sinuosity of 1.1, and an average longitudinal slope of 21% (Natural Resources Conservation

106 Service).

107
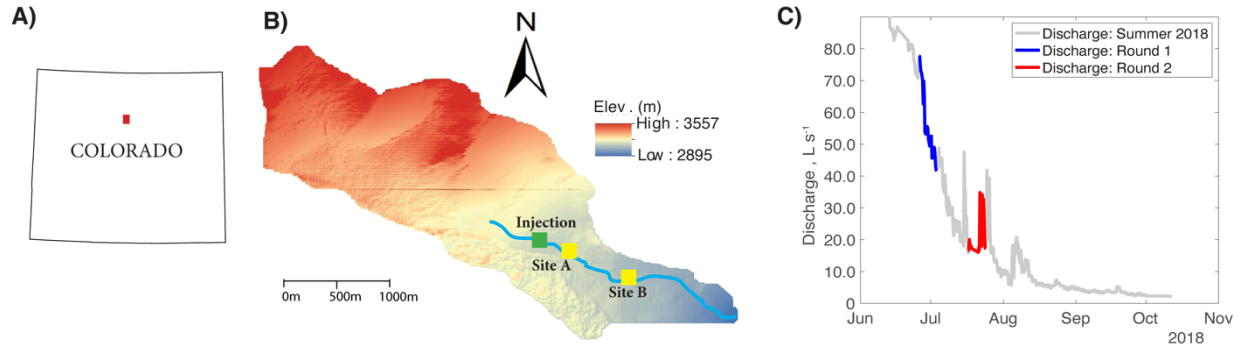
Figure 1: A) Location of Como Creek watershed in Colorado, B) detailed map of the watershed where Sites A and B are 50 and 350 m downstream from the injection location, and C) hydrograph and timing of experimental work; each round of experiments consisted of four treatments featuring N, N+C, N+P, and C+N+P nutrient additions.

2.2 Stream tracer injection experiments

We conducted two rounds of experiments, each consisting of four sets of continuous injections (lasting ~ 4-7 h) of Cl^- as a conservative tracer, resazurin (referred to as Raz hereafter) as a proxy for aerobic respiration, and one of the following nutrient treatments: a) N, b) N+C, c) N+P, and d) C+N+P. In our study, the nutrient treatments are treated as known system modifications (control variables) to alter metabolism. Also, we use the transformation of Raz, which occurred at the same spatiotemporal scales of the nutrient additions, to calculate how changes in stoichiometric conditions and discharge affect respiration. Briefly, the reactive tracer Raz (blue in color) is irreversibly reduced to resorufin (Rru, red) under aerobic respiration, and the relationship between Raz transformation and oxygen consumption is linear (González-Pinzón et al. 2012, 2014, 2016; Knapp et al. 2018; Dallan et al. 2020).

Before each tracer injection, we used the Tracer Injection Planning Tool (TIPT) (González-Pinzón et al. 2022) to estimate the amount of tracer mass needed to reach steady state conditions at the downstream site and to estimate the duration of the tracer breakthrough curves. From our field sampling, ambient concentrations of nitrate averaged 0.035 (±0.002) mg/L. We corroborated this value with a study by (Smith et al. 2003), who generated estimates of background total nitrogen (TN) and total phosphorous (TP) yield and concentrations throughout the stream-river network in 14 ecoregions of the conterminous US. That study found 75th % quartile TN= 0.21 (±0.05) mg/L and TP= 0.02 (±0.005), which indicates relatively low nutrient concentrations compared to agricultural streams in the US Midwest featuring ambient concentrations of up to two orders of magnitude higher. Based on estimated discharges and reach lengths, we targeted a maximum concentration of 2 mg/L for Cl, and 100 µg/L at the most downstream locations. The concentrations for nitrogen, phosphorus, and carbon were based on the expected detection limit of phosphate (i.e., 0.1 mg/L) for common ion chromatographs. From that minimum phosphate concentration expected, we scaled the masses of nitrogen and carbon using the 106C:16N:1P Redfield ratio (Redfield, 1934). Table 1 shows the masses injected and the discharges observed during the studies. Note that we allowed the stream to return to ambient concentrations for one day after each set of injections.

139

Table 1: Tracer injection data for each round of experiments at Como Creek.

Date	Treatment	Discharge (L/s)	Start time	End time	NaCl (g)	KNO$_3$ (g)	KPO$_4$ (g)	Sodium Acetate (g)	Raz (g)
Round 1									
6/26/18	N	74	11:30	17:00	32653	502	-	-	150
6/28/18	N+C	61	10:08	14:10	32680	500	-	2000	150
6/30/18	N+P	53	10:00	17:00	32680	500	400	-	150
7/2/18	C+N+P	49	9:59	14:00	32680	500	400	2000	150
Round 2									
7/17/18	N	20	10:30	14:35	10000	100	-	-	30
7/19/18	N+C	17	10:00	13:59	10000	100	-	400	30
7/21/18	N+P	17	10:00	14:06	10000	100	80	-	30
7/23/18	C+N+P	25	9:30	13:35	10000	100	80	400	30

140

141   We collected 20 mL aliquots in each tracer injection 50m and 350m downstream of the injection site

142   (labeled Sites A and B, Figure 1) to generate tracer breakthrough curves (BTCs) for Raz. All samples were filtered

143   immediately after being collected using a 0.7 µm GF/F filter (Sigma-Aldrich) and kept on dry ice during transport

144   until they were frozen at -4°C for laboratory analysis for Raz concentrations. All analyses took place within a week

145   after the end of each round of injections. At the laboratory, each sample was buffered to a pH of 8.5 (1:10 buffer-to-

146   sample) following Knapp et al. (2018). The fluorescence signals were measured with a Cary Eclipse Fluorescence

147   Spectrophotometer (Agilent Technologies) using excitation/emission wavelengths of 602/632 nm for Raz and

148   571/584 nm for Rru and converted to concentrations based on an 8-point calibration curve (R^2=0.99).

149   We monitored specific conductivity (SC) and temperature using Campbell Scientific CS547A sensors

150   connected to Campbell Scientific CR 1000 dataloggers, which recorded and stored those measurements every 10

151   minutes. From the grab samples, we measured chloride using a Dionex ICS-1000 Ion Chromatograph with

152   AS23/AG23 analytical and guard columns. Cl data were augmented with background-corrected SC data to model

153   conservative transport.

154   We monitored changes in stream stage every 10 minutes at the end of the study reach using pressure

155   transducers (Campbell Scientific CS420) connected to a datalogger (Campbell Scientific CR 1000). We used

156   established stage-discharge relationships specific for the study site, as provided by the site managers. The discharge

157   values reported in Table 1 represent mean values observed during a given experiment.

158   **2.2 Conservative transport modelling and metrics**

159   We calibrated the conservative transport parameters of the transient storage model presented in Equations 1

160   and 2 using Cl$^-$ and streamwater electrical conductivity data observed at Sites A and B. For this, we used the Matlab

161   (The Mathworks Inc., Natick, Massachusetts) script from Knapp et al. (2018), which features a joint calibration of

162   conservative and reactive solutes through a non-linear, least squares optimization routine.

163    $\frac{\partial c}{\partial t} = -u\frac{\partial c}{\partial x} + D\frac{\partial^2 c}{\partial x^2} - \frac{A_s}{A}\frac{\partial c_{ts}}{\partial t} + q_{in}c - \lambda_{mc}c$ (1)

164    $\frac{\partial c_{ts}}{\partial t} = k(c - c_{ts}) - \lambda_{ts}c_{ts}$ (2)

165

166 where c [ML^{-3}] and, c_{ts} [ML^{-3}] are the concentrations in the main channel and aggregate transient storage zone; x

167 [L] is the distance of the study reach; t [T] is time; u [LT^{-1}] and D [L^{2}T^{-1}] are parameters representing advective

168 flow velocity and dispersion coefficient, respectively; q_{in} [T^{-1}] is a volumetric flux parameter accounting for lateral

169 inputs; $k[T^{-1}]$ is the first-order mass transfer rate coefficient parameter between the main channel and the aggregate

170 transient storage zone; A_s/A [$-$] is the capacity ratio parameter representing the relative contribution of transient

171 storage-dominated to advection-dominated compartments in the stream, represented as areas along the reach; and

172 λ_{mc} and λ_{ts} [T^{-1}] are processing-rate coefficients in the main channel and transient storage zones (equaling zero for

173 a conservative tracer).

174   We completed the parameter estimation using the Differential Evolution Adaptive Metropolis (DREAM

175 [ZS]) algorithm (Vrugt et al. 2009). We jointly fit Cl− and Raz data in a first step of 100,000 model generations. We

176 assessed model convergence using Gelman and Rubin $\hat{R}$ statistics (Gelman and Rubin 1992). The goodness of fit

177 between measured and simulated BTCs was quantified through the calculation of the residual sum of squares,

178 (nRSS) (–), normalized by the squared theoretical peak tracer concentrations of each tracer BTC of the respective

179 tracer at the given location. The medians of the best 1,000 model simulations were used to assess the agreement

180 between our final model fits and a subset of possible curve fits. The details on the model calibration procedure that

181 we use in this work were presented in the supporting information of Gootman et al. (2020). Examples of observed

182 and fitted breakthrough curves can be found in Figures S1-S3.

183   We estimated conservative transport timescales from the transport parameters to describe the transient

184 storage timescale, $\tau_{sz} = 1/k$ [T], and the mean travel time between sites A and B, τ [T], which was computed as:

185 $\tau = \frac{m_{1,cl}}{m_{0,cl}}$ (3)

186 $m_n = \sum_{i=1}^{r} \left(\frac{t_i+t_{i+1}}{2}\right)^n \left(\frac{C_i+C_{i+1}}{2}\right)(t_{i+1} - t_i)$ (4)

187 where $m_{0,cl}$ and $m_{1,cl}$ are the zeroth and first-centralized temporal moments of the Cl$^-$ BTCs from each sampling

188 site, i is a time index, r is the total number of samples available in a BTC.

189 **2.3 Estimating the transformation of Raz as a proxy for microbial respiration:**

190   We used the net transformation rate coefficients of Raz, λ_{Raz} [T^{-1}], as a proxy for microbial respiration~.~.

191 λ_{Raz} incorporates transformation in the main channel and in transient storage zones, and was estimated ~and~

192 ~estimated them~ following the work by González-Pinzón and Haggerty (2013), ~which~ who derived algebraic

193 relationships with analytical solutions to calculate processing rate coefficients from the transient storage model

194 presented in Equations 1 and 2:

195 $\lambda_{Raz} = \frac{\ln(m_{0,Raz}^{inj}/m_{0,Raz}^{BTC})}{\tau}\left(1 + \frac{\overbrace{\ln(m_{0,Raz}^{inj}/m_{0,Raz}^{BTC})}^{dispersion\ term, \Phi}}{Pe}\right)$ (5)

196 where $m_{0,Raz}^{inj} = M_{Raz}/Q$ is the zeroth temporal moment of Raz at the injection site [M L^{-3} T^{-1}], M_{Raz} is the mass of

197 Raz added to the injectate, Q is the stream discharge [L^{3}T^{-1}]; $m_{0,Raz}^{BTC}$ is the dilution-corrected zeroth temporal

198 moment of Raz estimated with BTC data from a sampling site; and $Pe = L\,u/D$ is the Peclet number [-], which

199 describes the relative importance of advection and dispersion in the system. As noted by González-Pinzón and

200 Haggerty (2013), when $Pe \gg 10$, which is the case in advection-dominated systems such as open channel flow, the

201 dispersion term Φ is negligible and $\lambda_{Raz} \approx \ln(m_{0,Raz}^{inj}/m_{0,Raz}^{BTC})/\tau$.

202 Since we can only get one ~~processing~~transformation- rate coefficient from every observed BTC available

203 from Equation (5), or from the direct calibration of the transient storage model, we ~~expanded the work by González-~~

204 ~~Pinzón and Haggerty (2013) to incorporate the conceptual principles proposed in the~~used the Tracer Addition for

205 Spiraling Curve Characterization (TASCC) framework (Covino et al. 2010b)~~, where multiple rate coefficients can~~

206 ~~be estimated from an equivalent version of Equation 5.~~

207 ~~Briefly, TASCC uses the dynamic range of solute concentrations sampled in BTCs~~ to characterize uptake

208 kinetics over the range of experimental concentrations observed ~~from ambient to saturation concentrations~~. In

209 TASCC, the ratio of reactive to conservative solute concentrations for every independent sample across the tracer

210 BTCs is compared to the ratio of the concentrations of the injection solution to determine uptake metrics. If the

211 added solutes are non-reactive, they will transport conservatively, and the ratio of the reactive to conservative solute

212 concentrations will remain constant. Alternatively, if the added solutes are limiting, co-limiting or reactive, they will

213 not transport conservatively, and the ratio of the reactive to conservative solute concentrations will change over time

214 as a function of reactivity.

215 ~~To incorporate the TASCC framework into the algebraic equation developed by González-Pinzón and~~

216 ~~Haggerty (2013) and estimate transformation rate coefficients for Raz from each pair of conservative (i.e., $C_{cons.}$)~~

217 ~~and reactive tracer concentrations (i.e., C_{Raz}), we need to replace m_u with $C_{Raz}/C_{cons.}$ This guarantees that the mean~~

218 ~~value of all the processing rate coefficients is equal to the processing rate coefficient estimated from the zeroth~~

219 ~~temporal moment analysis of model-derived simulations from Equations (1) and (2).~~TASCC-based transformation

220 rate coefficients for Raz were estimated using ~~Accordingly~~:

221
$$\lambda_{Raz,sample} = \frac{\ln\left[\frac{C_{Raz}}{C_{cons.}}\right]_{inj} - \ln\left[\frac{C_{Raz}}{C_{cons.}}\right]_{BTC}}{\tau x/u} \left(1 + \overbrace{\frac{\ln\left[\frac{C_{Raz}}{C_{cons.}}\right]_{inj} - \ln\left[\frac{C_{Raz}}{C_{cons.}}\right]_{BTC}}{Pe}}^{dispersion\ term,\Phi}\right).$$

222 (6)

223 ~~Equation 6 directly links different transport mechanisms used to explain the transport and fate of solutes~~

224 ~~(i.e., advection, dispersion, transient storage, and reactivity) with TASCC, an algorithm yielding higher information~~

225 ~~content from experimental work. We note here that alternative forms of Equation 6 can be derived for solute~~

226 ~~transport models, including additional reactions such as sorption and production. Therefore, similar new equations~~

227 ~~could be derived to provide mechanistic explanations to TASCC-related findings noticing hysteresis behavior in~~

228 ~~nutrient uptake between the rising and falling limbs of experimental BTCs (Gibson et al. 2015; Trentman et al.~~

229 ~~2015; Rodríguez-Cardona et al. 2016; Brooks et al. 2017; Day and Hall 2017).~~ Finally, ~~f~~From each transformation

230 rate coefficient λ_{Raz} and $\lambda_{Raz,sample}$, we also estimated an uptake (or mass transfer) velocity of Raz, $V_{f_{Raz}} = \lambda_{Raz}h$

231 or $V_{f_{Raz,sample}} = \lambda_{Raz,sample}$ -h, where h is the mean depth of the stream. Following Ensign and Doyle (2006),

232 uptake velocities represent the vertical velocity of solute molecules through the water column towards the benthos

233 and are typically used in stream ecology to normalize processing-rate coefficients by the influence from contrasting

234 discharge magnitudes to facilitate the comparison of results from small streams and large rivers. As demonstrated in

235 Covino et al. (2010b), the range of $\lambda_{Raz,sample}$ and $V_{f_{Raz,sample}}$ values encompass the λ_{Raz} and $V_{f_{Raz}}$ values

236 obtained from processing rates derived from temporal moments analyses (e.g., Equation (5)).

237   Finally, reach-scale Damköhler numbers, Da [-], were calculated using the following equation:

238 $$Da = \frac{transient\ storage\ timescale}{transformation\ timescale} = \tau_{sz}\lambda_{Raz}. \qquad (7)$$

239 **2.4 Statistical tests**

240   We calculated standard deviations (std) based on repeated measures of the distribution of the transport

241 parameters of Equations 1 and 2 to create upper and lower boundaries of the uncertainties in our measurements (i.e.,

242 mean ± std). Because our data were not normally distributed, we used the Mann-Whitney U nonparametric statistical

243 test to determine if there were statistically significant differences between nutrient treatments across rounds (e.g., N

244 vs. N in rounds 1 and 2), following a similar procedure in Ensign and Doyle (2006). For the Mann-Whitney U test,

245 we set our significance level (α, alpha) equal to 0.05.

246   We explored the Pearson correlation coefficient (r) matrix between the transport parameters of Equations 1

247 and 2, and associated metrics, to establish direct ($r > 0.1$), inverse ($r < -0.1$), and non-existent correlations ($-0.1 < r$

248 < 0.1) (Bowley 2008). We classified the strength of the correlations as uncorrelated ($0 < r < |0.1|$), weakly correlated

249 ($|0.1| < r < |0.5|$), moderately correlated ($|0.5| < r < |0.8|$), strongly correlated ($|0.8| < r < |1.0|$), and included p-values for

250 each correlation.

251   Lastly, we tested differences in mean values of the transport parameters of Equations 1 and 2, and

252 associated metrics, between nutrient treatments within each experimental round (e.g., N vs. N+C vs. N+P vs.

253 C+N+P in round 1) using the Student's t-test based on deviation from the group's mean value (Blair et al. 1980).

254 **3 Results and Discussion**

255 **3.1 Conservative transport and metrics of physical controls**

256   Between experimental rounds 1 and 2, stream depth (h) and discharge (Q) decreased, causing significant

257 differences in stream velocity (u), dispersion (D), mass-transfer rate coefficients (k), transient storage time scales

258 (τ_{TS}) and mean travel times (τ) (Figure 2). The only parameter that did not show significant differences was the

259 relative contribution of the main channel to storage zone areas, A_s/A.

260
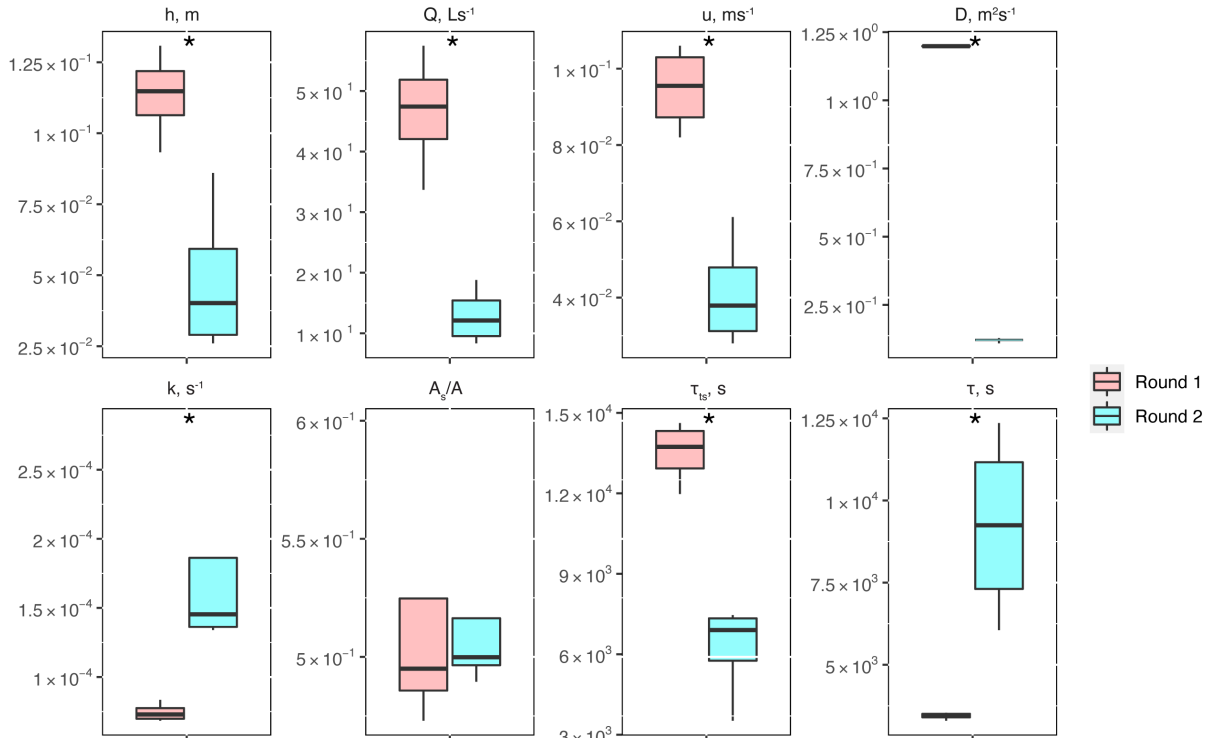
Figure 2: Conservative transport parameters and metrics of physical controls estimated for the two experimental rounds: stream depth (h), stream velocity (u), dispersion (D), mass transfer rate coefficients (k), the ratio of transient storage-dominated to advection-dominated compartments (A_s/A), transient storage time scales (τ_{TS}) and mean travel times (τ). Asterisks represent statistical differences in magnitudes for rounds 1 and 2 with $p<0.05$ (*) based on the Mann-Whitney U nonparametric statistical test.

The correlation matrix between parameters and metrics (Figure 3) shows that Q (and interrelated quantities h and u), D, and τ_{ts} were all directly correlated (from moderately to strongly). Mean travel times between sites, τ, were directly and weakly correlated with k and the ratio A_s/A, and inversely correlated (from weakly to strongly) with the rest of the conservative transport parameters and metrics. Finally, the ratio A_s/A was generally uncorrelated or weakly correlated with other quantities. Even though the correlations of some interdependent quantities are known to be spurious, e.g., Q vs. u and λ_{Raz} vs. $V_{f_{Raz}}$ (González-Pinzón et al. 2015), we included all relevant measured and modeled quantities in Figure 3 to allow readers to explore different data pairs. For clarity, we differentiate with brackets all known spurious correlations. Note that we did not flag the correlation between A_s/A and Q (and their interrelated quantities h and u) as spurious because the ratio of areas is an indicator of the relative volume-based contribution from advection-dominated to transient storage-dominated compartments, instead of actual estimates of cross-sectional areas (Kelleher et al. 2013; González-Pinzón et al. 2013; Knapp and Kelleher 2020).
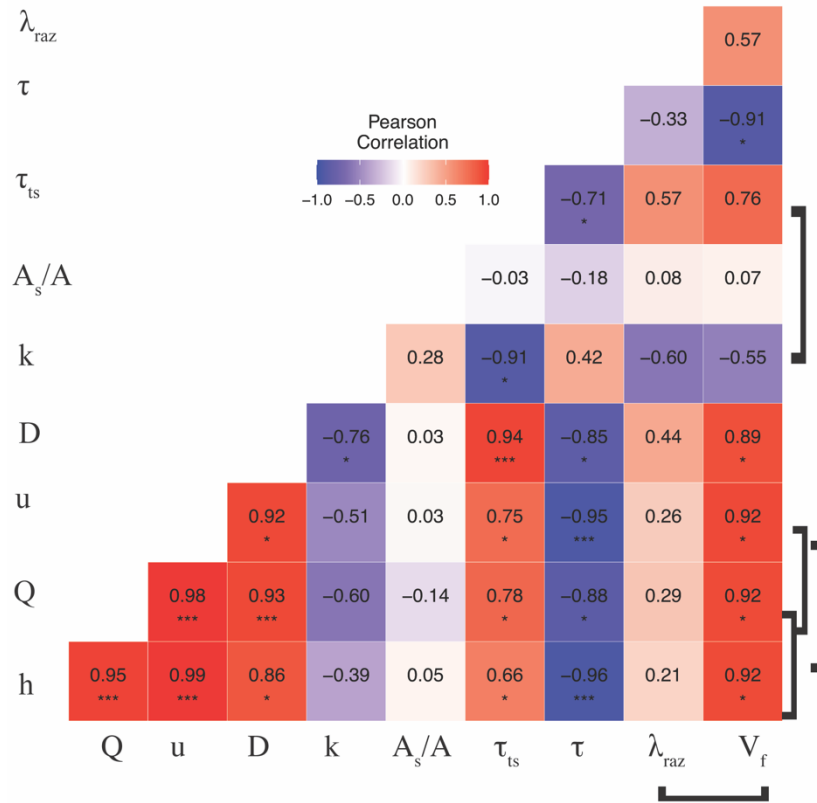
Figure 3: Pearson correlation coefficient (r) heatmap for the mean values of the transport parameters and metrics for each stoichiometric treatment during rounds 1 and 2. Brackets link known spurious correlations. Asterisks represent significant differences in magnitudes between parameters with p<0.05 (*), and p<0.001(***) based on the Pearson Correlation.

One of the metrics of interest in stream reactive-transport modeling is the transient storage timescale ($\tau_{ts} = 1/k$), which quantifies the exposure that solutes have to biological communities in metabolically active transient storage zones. In our study site, τ_{ts} decreased one order of magnitude from round 1 to round 2, and were comparable to the range of values observed in other studies involving forested mountain streams (Valett et al. 1996; Hall et al. 2002). Due to the geomorphology of the stream, which is characterized by pool and riffle sequences, but steep longitudinal and valley slopes and shallow bedrock, transient storage was expected to occur mainly in the main channel (Fields and Dethier 2019; Barnhart et al. 2021; Emanuelson et al. 2022). As flow receded from round 1 to round 2, we observed the disconnection of in-stream pools contributing to transient storage, which explains the direct correlation between discharge and transient storage timescales. Another indication of the dominant contribution of in-stream pools to total transient storage is the lack of change of A_s/A with discharge. Since A is expected to vary proportional with discharge (i.e., $Q = A \cdot u$), a constant A_s/A suggests that the contribution of transient storage-dominated (i.e., A_s) compartments (i.e., A) also varied proportionally with discharge.

**3.2 Raz transformation (a proxy for respiration) as a function of physical controls**

Our results indicate that the mean values of the transformation rate coefficient of Raz (λ_{Raz}) were directly and moderately correlated with the transient storage timescale (τ_{ts}), as other studies on reactive transport have

10

302 shown (Valett et al. 1996; Hall et al. 2002; Gomez et al. 2012; Zarnetske et al. 2012; Kiel and Bayani Cardenas
303 2014; Gootman et al. 2020). Mean λ_{Raz} values were directly and weakly correlated with discharge (Q) (also depths
304 h and velocities u) and dispersion (D), and directly and moderately correlated with τ_{ts}. Mean λ_{Raz} values were
305 inversely and weakly correlated with mean travel times (τ), and inversely and moderately correlated with mass-
306 transfer rate coefficients (k) (Figure 3). Raz uptake velocities ($V_{f_{Raz}}$) showed spurious, direct and strong
307 correlations with discharge (Q) (also h and u), strong correlations with dispersion (D) and transient storage
308 timescales (τ_{ts}), and strong indirect correlations with mean travel times (τ) and k (moderate). Finally, both λ_{Raz} and
309 $V_{f_{Raz}}$ were uncorrelated with A_s/A. Unlike studies where an increased transient storage timescale (τ_{ts}) is mainly
310 associated with slower hyporheic flows due to lower discharges (Q) (Zarnetske et al. 2007; Schmid et al. 2010), τ_{ts}
311 in our study site increased with Q because the geomorphology of the channel and the valley favored in-stream
312 transient storage in lateral pools (Jackson et al. 2012, 2013, 2015). Similar declines in transient storage with falling
313 discharge have been observed in other streams with comparable geomorphic characteristics (Covino et al. 2010a;
314 Emanuelson et al. 2022), however, the absence of concurrent declines in respiration suggest biological control by
315 some other mechanism.

316 **3.3 Raz transformation (a proxy for respiration) as a function of physical and stoichiometric controls**

317 Our results suggest no significant changes in respiration despite significant differences in discharge (Q),
318 temperature, and nutrient treatments. Between experimental rounds, the mean values of Q (and h and u by
319 extension) and temperature (except for N+C) were statistically different for each treatment comparison (Figure 4A).
320 For $\lambda_{Raz,sample}$, we only found statistical differences between rounds for the C+N+P treatments (Figure 4C). Due to
321 the large influence of Q on the uptake velocity of Raz ($V_{f_{Raz,sample}}$) through stream depth (h), the statistical
322 differences between rounds seen for Q were also seen for $V_{f_{Raz,sample}}$ (Figure 4D).

323

324

325
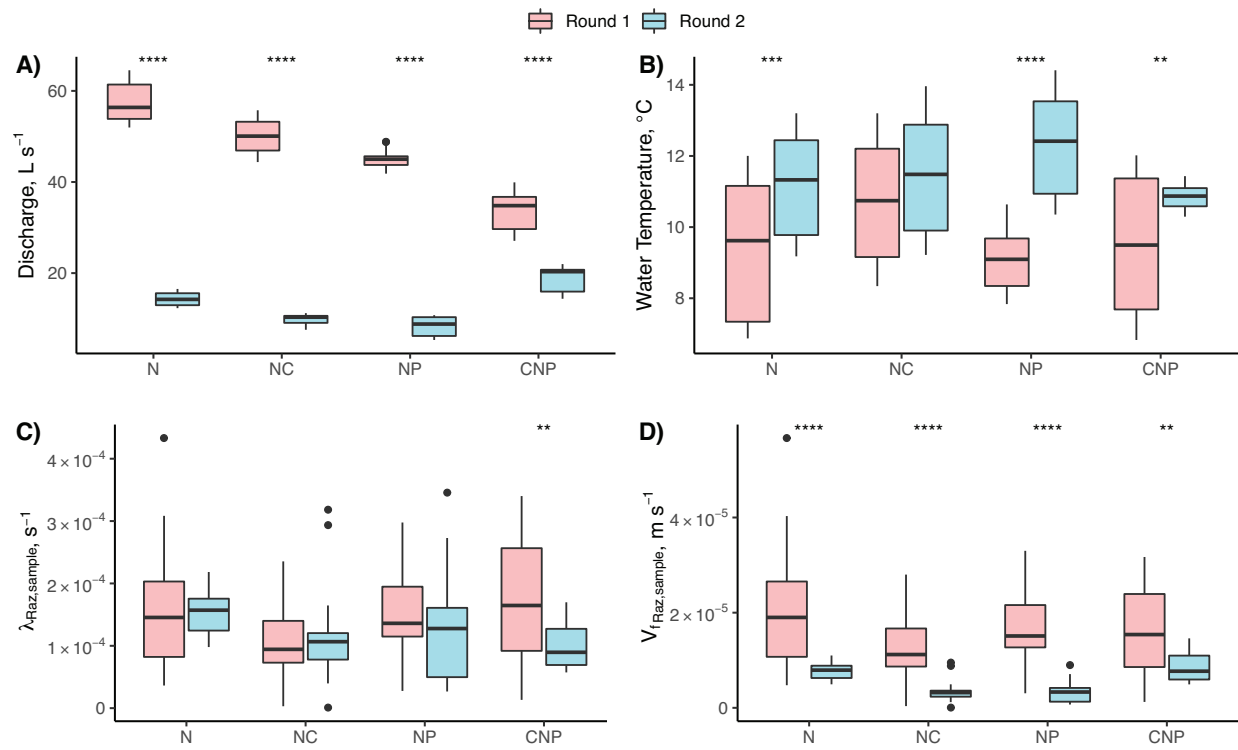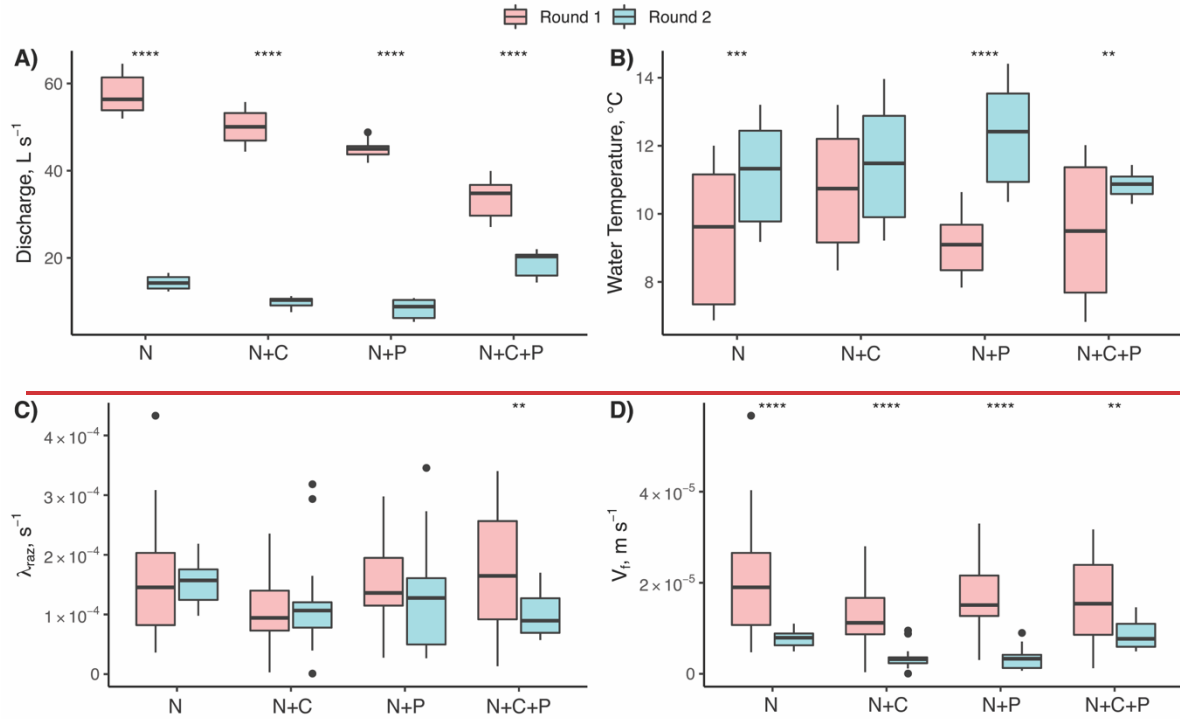
326 **Figure 4: Comparison of A) stream discharge values recorded at the gaging station, B) stream water temperatures, C)**
327 **transformation rate coefficients of resazurin ($\lambda_{Raz,sample}$) resulting from Equation 6, and associated D) uptake velocities**
328 **of resazurin ($V_{f_{Raz,sample}} = \lambda_{Raz,sample}\ h$) estimated for each experimental nutrient treatment addition during rounds 1**
329 **and 2. Due to the large influence of Q on the uptake velocity of Raz ($V_{f_{Raz,sample}}$) through stream depth (h), most of the**
330 **statistical differences between rounds seen for Q were also seen for $V_{f_{Raz,sample}}$. Asterisks represent significant**

331 **differences in magnitudes between rounds with p<0.01(**), and p~0 (****) based on the Mann-Whitney U nonparametric**
332 **statistical test.**

333
334   When looking at the data collected from each round, we found that mean Q values were statistically

335 different across nutrient treatments (Figures 5A and 5D). For mean $\lambda_{Raz,sample}$ values, the only treatments with

336 statistical differences were the N+C and C+N+P from round 1 (Figures 5B and 5E). Finally, $V_{f_{Raz,sample}}$ mean

337 values were only statistically different for the N vs N+C treatments for round 1, and for all but the N+C vs N+P and

338 N vs C+N+P treatments for round 2 (Figures 5C and 5F).

339
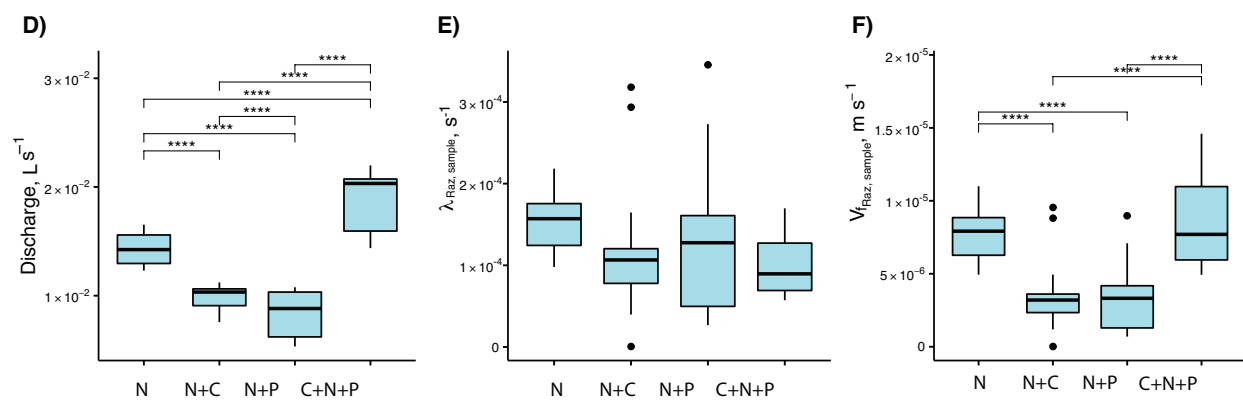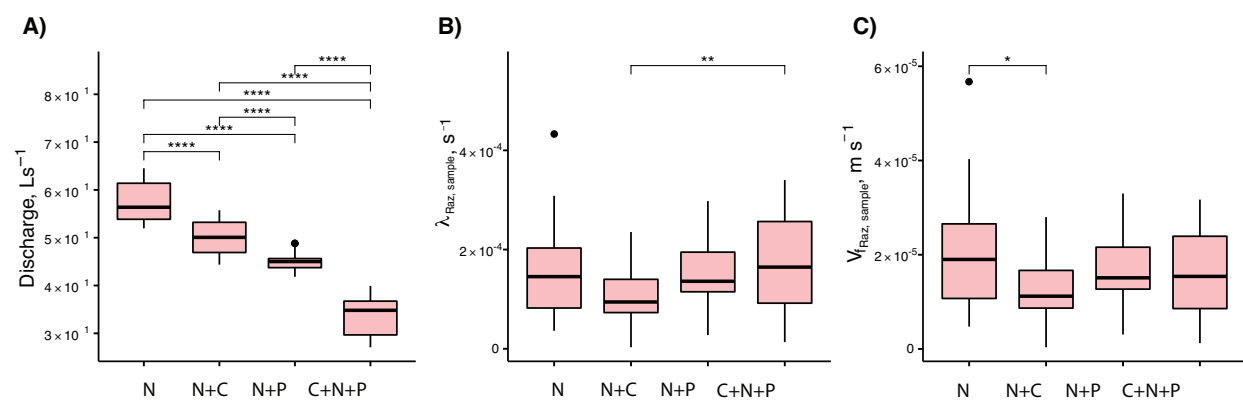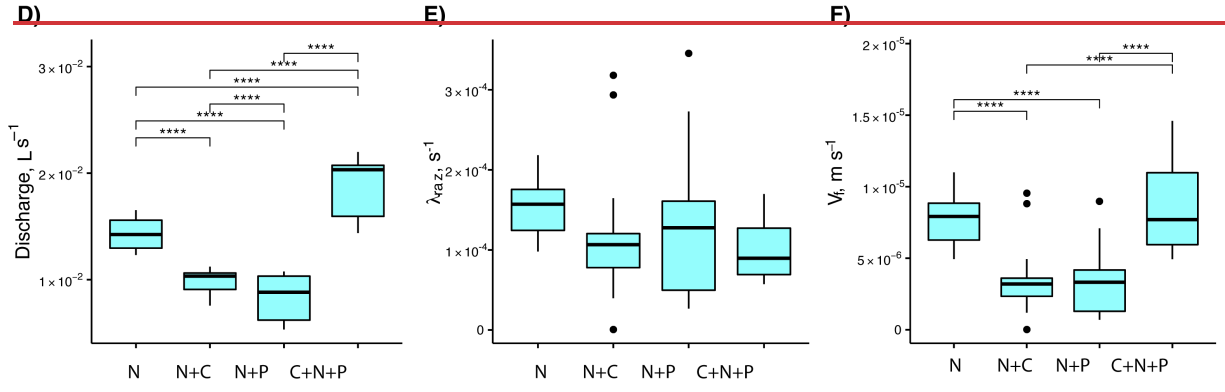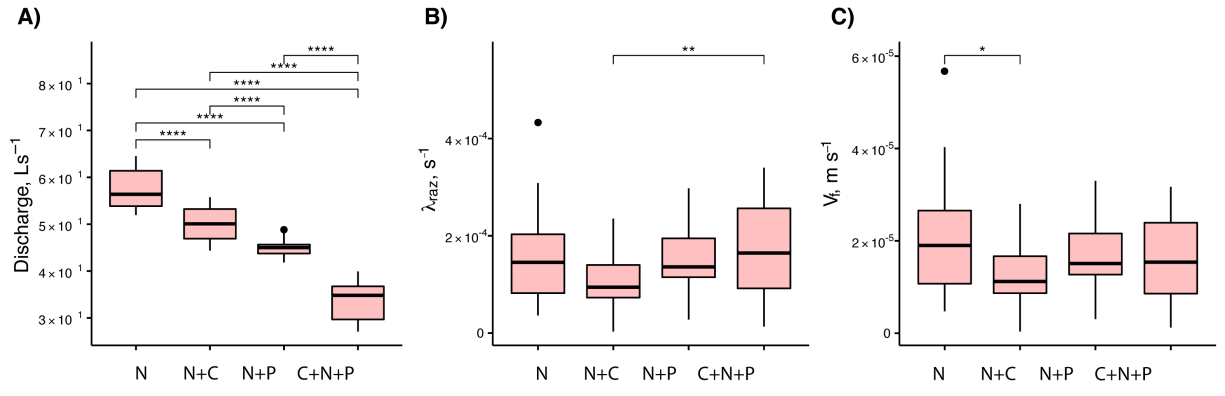
Figure 5: Comparison of stream discharges (A and D), transformation rate coefficients of resazurin ($\lambda_{Raz,sample}$) resulting from Equation 6 (B and E), and associated uptake velocities of resazurin ($V_{f_{Raz,sample}}$) (C and F) across treatments for round 1(top row) and 2 (bottom row). Due to the large influence of Q on the uptake velocity of Raz ($V_{f_{Raz,sample}}$) through stream depth (h), most of the statistical differences between rounds seen for Q were also seen for $V_{f_{Raz,sample}}$. Asterisks represent significant differences in magnitudes for treatments N, N+C, N+P, and C+N+P with p<0.05 (*), p<0.01(**), and p~0 (****) based on the Mann-Whitney U nonparametric statistical test.

For each of the eight nutrient injections, we related the mean transient storage timescales, τ_{ts}, which indicate exposure times between solutes and microbial communities, and the mean transformation timescales of Raz, $1/\lambda_{Raz}$, which indicate respiration (Figure 6). This Damköhler-based analysis allows us to visualize the interplay between physical, biological, and stoichiometric controls in the stream. We found that the range of variation of the mean transient storage timescales was three times greater than that of the mean transformation timescales. In round 1, all the stoichiometric treatments resulted in transport-limited conditions due to the high values of τ_{ts}, i.e., the average particle of Raz that entered a metabolically active compartment underwent transformation and more Raz could have been transformed if it had been available. Thus, in round 1, respiration was high relative to the supply of solutes to the metabolically active transient storage zones. In round 2, all stoichiometric treatments, except N, resulted in reaction-limited conditions, i.e., the average particle of Raz entering a metabolically active compartment left it without undergoing transformation. Thus, in round 2, respiration was slow relative to the exposure of solutes to microbial communities.
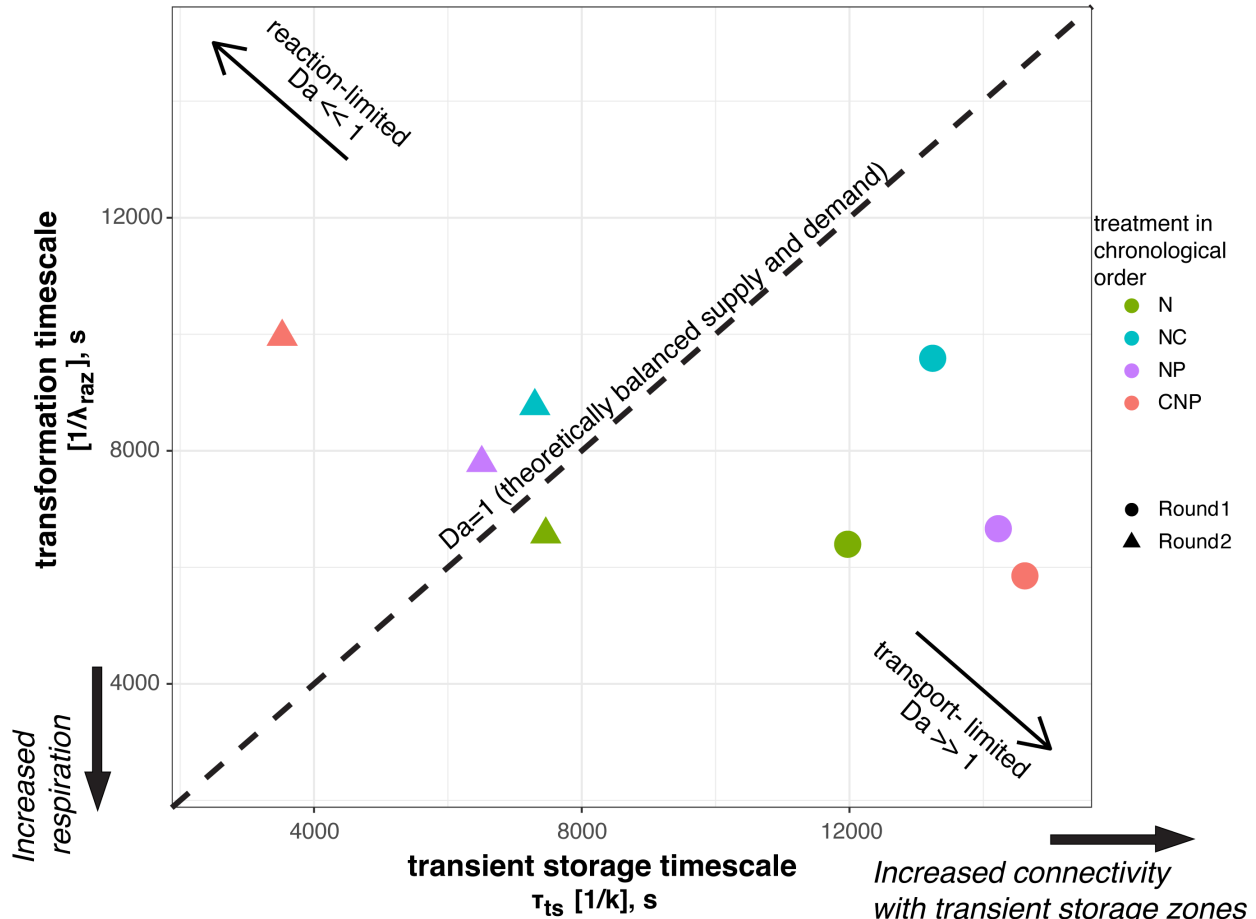
Figure 6: Mean reaction and transient storage timescales for each nutrient treatment. The Damköhler, $Da =$ transient storage timescale/ transformation timescale, indicates reaction-limited and transport-limited conditions.

3.4 How is microbial respiration controlled by hydrologic exchange vs. stoichiometric conditions (i.e., supply of C, N, and P)?

We characterized microbial respiration with the transformation timescale of Raz, $1/\lambda_{Raz}$; the extent of hydrologic exchanges with the transient storage timescale, τ_{TS}, and the relative size of the main channel and transient storage areas, A_s/A; and stoichiometric conditions with our controlled nutrient additions (i.e., N, N+C, N+P, and C+N+P treatments). The most salient findings indicate that a) discharge (Q) changed significantly between rounds (Figure 4a) and across stoichiometric treatments (Figure 5a, 5d), and was directly and moderately correlated with τ_{TS} and uncorrelated with A_s/A (Figure 3), suggesting that most transient storage occurred in lateral pools in the channel, which increased in quantity and extent proportionally with Q, and b) the respiration activity indicated by λ_{Raz} remained similar between rounds with significantly different Q (Figure 4b), and across controlled stoichiometric treatments also featuring different Q (Figure 5b, 5e). Thus, we observed that respiration remained largely unchanged or constant with varying physical and stoichiometric conditions.

Several hypotheses may explain the invariant respiration observed between experimental rounds and treatments. First, tradeoffs in metabolic rates may have occurred as the stream shifted from high to low flows. At

16

high flows during late June and early July, lateral pools in the main channel were inundated, and transient storage timescales likely associated with these pools were high. Under these conditions, the observed respiration was probably supported by low levels of processing in the hyporheic zone due to the prevalence of bedrock substrate and relatively low respiration from benthic biomass due to scour from high flows (Francoeur and Biggs 2006; Katz et al. 2018). However, the combination of longer transient storage timescales and an expanded total surface area resulted in moderate total respiration. In contrast, during the low flows seen in the second round of injections, surface area, and transient storage timescales were decreased due to the contraction of the channel. Under these conditions, biomass increased likely due to decreased scour and increased stability (Francoeur and Biggs 2006; Katz et al. 2018; Cargill et al. 2021), increased water temperatures (Perkins et al. 2012), and increased processing of autochthonous carbon (Wagner et al. 2017) (Figure S4). This may have supported elevated areal metabolic rates in benthic biofilms (Battin et al. 2016), maintaining relatively constant respiration levels with respect to the first round of injections.

An alternative hypothesis to explain the consistency of the observed respiration values is that some other factor constraints respiration values within a narrow range. For example, the limitation of a key nutrient or metabolic resource may constrain respiration. While we designed the experiments to relieve stoichiometric constraints, it is possible that the quantities of C, N, and P in the injectate we were logistically able to introduce to the stream were insufficient to overcome demand. Also, the form of the resources may not have been readily available to communities adapted to these locals, as stream microbial communities most efficiently process the forms and diversity of dissolved organic matter found in their native habitats, and they express extracellular enzymes in ratios appropriate to acquire limiting nutrients (Hill et al. 2012; Lane et al. 2012; Wilhelm et al. 2015; Logue et al. 2016).

In previous studies, transient storage and nutrient uptake have presented contradictory relationships, which we summarize below.

Inconclusive relationships: Martí et al. (1997) did not find correlations between NH_3 uptake length and A_s/A in a desert stream using data from eight tracer injections. Webster et al. (2003) did not find statistically significant relationships between NH_4 uptake and A_s/A using the 11-stream LINX-I dataset that included arctic to tropical streams. From thirty seven injections conducted in thirteen streams at Hubbard Brook Experimental Forest (HBEF), Hall et al. (2002) found weak correlations (R^2=0.14-0.35) between transient storage parameters and NH_4 demand. Using data from seven streams in New Zealand, Niyogi et al. (2004) did not find significant correlations between soluble reactive phosphorous (P-SRP), NO_3 uptake velocities, and A_s/A. Bukaveckas (2007) reported an indefinite relationship between transient storage and NO_3 and P-SRP retention efficiencies from tracer injections in a reference (N=13 injections), a channelized (N=14 injections), and a restored (N=17 injections) stream reach in the midwestern US. Lastly, the LINX-II dataset from ^{15}N-NO_3 injections in 72 streams located in eight regions of the US showed no relationship between NO_3 uptake and the fraction of median travel time due to transient storage (F_{med}^{200}) (Hall et al. 2009).

Weak to moderate relationships: Thomas et al. (2003) showed that transient storage accounted for 44% to 49% of NO_3 retention measured by ^{15}N in a small headwater stream in North Carolina. Mulholland et al. (1997) found larger PO_4 uptake rates in a stream with higher transient storage, when they compared two forested streams. Ensign and Doyle (2005) found an increase in A_s/A and the uptake velocities for NH_4 and PO_4 after the addition of

418   flow baffles to two streams. Lautz and Siegel (2007) found a modest correlation (R^2=0.44) between NO_3 retention

419   efficiency and transient storage in the Red Canyon Creek watershed, WY.

420   *Strong relationships:* Valett et al. (1996) found a strong correlation (R^2=0.77) between transient storage

421   and NO_3 retention in three first-order streams in New Mexico. From nine tracer injections in two urban streams in

422   the eastern US, Ryan et al. (2007) found strong relationships between P-SRP retention and transient storage metrics

423   ($k, A_s/A$; R^2>0.84) when the variables were measured in different seasons. Sheibley et al. (2014) observed that the

424   retention of NO_3 in seven agricultural streams in the US was positively correlated with A_s/A and the average water

425   flux through the storage zone per unit length of stream ($q_s = kA$), and negatively correlated with the transient

426   storage timescale (τ_{ts}). However, they found no significant correlation between NH_4^+ and SRP retention and

427   transient storage metrics.

428   The studies referenced above were performed in streams with contrasting physical, chemical, and

429   biological conditions. Together, they offer a broader perspective on the inconsistent relationship between transient

430   storage metrics and metabolic processing. Those studies do not feature co-injections of C, N, and P macronutrients

431   (e.g., N+C, N+P, N+C+P), even while some tracked ambient processing rates of more than one nutrient. Therefore,

432   they generally represent solute-specific analyses, where the uptake of one nutrient at a time was analyzed and, thus,

433   did not account for stoichiometric controls on nutrient uptake (however, see Tromboni et al. (2018) for an example

434   of recent trend changes in this research area). By combining both transport and stoichiometric analyses, our study

435   offers evidence that stoichiometric controls have an ambiguous relationship to reach-scale metabolic activities, and

436   that further investigations should be conducted using greater quantities and types of resources.

437   **4 Conclusions**

438   We conducted two rounds of four stoichiometric treatments (i.e., N, C+N, N+P, and C+N+P) in a

439   headwater stream in Colorado to quantify changes to stream respiration during flow recession and answer the

440   question: *How is respiration controlled by hydrologic exchange vs. stoichiometric conditions (i.e., supply of C, N,*

441   *and P)*? We found that discharge changed significantly between rounds and across stoichiometric treatments, and

442   that it was directly and moderately correlated with transient storage timescales but uncorrelated with the ratio of

443   contributions from advection-dominated to transient storage-dominated compartments (i.e., A_S/A). This suggests

444   that most transient storage occurred in lateral pools within the main channel, which increased in quantity and extent

445   proportionally with discharge. We also found that respiration remained similar despite significant changes in

446   discharge and stoichiometric treatments. Our results contradict the notion that hydrologic transport alone is a

447   dominant control on biogeochemical processing, and suggest that complex interactions between hydrology, resource

448   supply, and biological community function are responsible for driving in-stream respiration.

451 and prepared the manuscript with input from all co-authors. DVH supported the contextualization of hydrological and

452 ecological interactions. All co-authors approved the final version of the manuscript.

453 **Competing interests:** The authors declare no competing interests.

454 **Acknowledgments**

458 **Data availability:** The data used in his article can be found in the CUAHSI HydroShare repository. Gonzalez-Pinzon,
459 R. (2022). Resazurin tracer data from experiments in Colorado (2018) and Iowa (2019),
460 HydroShare, http://www.hydroshare.org/resource/50ae3c59bebe4cb383e31408a0c10012

461
462
463
464

465   **References**

466   Barnhart, T. B., J. Vukomanovic, P. Bourgeron, and N. P. Molotch. 2021. Future land cover and
467   climate may drive decreases in snow wind-scour and transpiration, increasing streamflow
468   at a Colorado, USA headwater catchment. Hydrol. Process. **35**: e14416.
469   doi:10.1002/hyp.14416
470   Battin, T. J., K. Besemer, M. M. Bengtsson, A. M. Romani, and A. I. Packmann. 2016. The
471   ecology and biogeochemistry of stream biofilms. Nat. Rev. Microbiol. **14**: 251–263.
472   doi:10.1038/nrmicro.2016.15
473   Battin, T. J., L. A. Kaplan, J. D. Newbold, and C. M. E. Hansen. 2003. Contributions of
474   microbial biofilms to ecosystem processes in stream mesocosms. Nature **426**: 439–442.
475   doi:10.1038/nature02152
476   Blair, R. C., J. J. Higgins, S. Journal, and N. Winter. 1980. A Comparison of the Power of
477   Wilcoxon ' s Rank-Sum Statistic to That of Student ' s t Statistic under Various
478   Nonnormal Distributions Published by : American Educational Research Association and
479   American Statistical Association Stable URL : https://www.jstor.org/stable/1164905
480   REFERENCES Linked references are available on JSTOR for this article : reference #
481   references _ tab _ contents You may need to log in to JSTOR to access the linked
482   references . **5**: 309–335.
483   Blume, E., M. Bischoff, J. M. Reichert, T. Moorman, A. Konopka, and R. F. Turco. 2002.
484   Surface and subsurface microbial biomass, community structure and metabolic activity as
485   a function of soil depth and season. Appl. Soil Ecol. **20**: 171–181. doi:10.1016/S0929-
486   1393(02)00025-2
487   Bowley, A. L. 2008. The Standard Deviation of the Correlation Coefficient Author (s): A . L .
488   Bowley Source : Journal of the American Statistical Association , Vol . 23 , No . 161 (
489   Mar ., 1928), pp . 31- Published by : American Statistical Association Stable URL :
490   http:/. J. Am. Stat. Assoc. **23**: 31–34.
491   Bukaveckas, P. A. 2007. Effects of Channel Restoration on Water Velocity, Transient Storage,
492   and Nutrient Uptake in a Channelized Stream. Environ. Sci. Technol. **41**: 1570–1576.
493   doi:10.1021/es061618x
494   Cardenas, M. B., J. L. Wilson, and V. A. Zlotnik. 2004. Impact of heterogeneity, bed forms, and
495   stream curvature on subchannel hyporheic exchange. Water Resour. Res. **40**: 1–14.
496   doi:10.1029/2004WR003008
497   Cargill, S. K., C. Segura, S. R. Villamizar, and D. R. Warren. 2021. The influence of lithology
498   on stream metabolism in headwater systems. Ecohydrology **14**. doi:10.1002/eco.2284
499   Covino, T. P., B. McGlynn, and M. Baker. 2010a. Separating physical and biological nutrient
500   retention and quantifying uptake kinetics from ambient to saturation in successive
501   mountain stream reaches. J. Geophys. Res. Biogeosciences **115**: 1–17.
502   doi:10.1029/2009JG001263
503   Covino, T. P., and B. L. McGlynn. 2007. Stream gains and losses across a mountain-to-valley
504   transition: Impacts on watershed hydrology and stream water chemistry. Water Resour.
505   Res. **43**: 1–14. doi:10.1029/2006WR005544
506   Covino, T. P., B. L. Mcglynn, and R. A. Mcnamara. 2010b. Tracer Additions for Spiraling Curve
507   Characterization (TASCC): Quantifying stream nutrient uptake kinetics from ambient to
508   saturation. Limnol. Oceanogr. Methods 484–498. doi:10.4319/lom.2010.8.484
509   Covino, T. P., B. McGlynn, and J. Mallard. 2011. Stream-groundwater exchange and hydrologic
510   turnover at the network scale. Water Resour. Res. **47**: 1–11. doi:10.1029/2011WR010942

511 Dallan, E., P. Regier, A. Marion, and R. González-Pinzón. 2020. Does the Mass Balance of the
512   Reactive Tracers Resazurin and Resorufin Close at the Microbial Scale? J. Geophys. Res.
513   Biogeosciences **125**: 1–10. doi:10.1029/2019JG005435
514 Emanuelson, K., T. P. Covino, A. S. Ward, J. Dorley, and M. N. Gooseff. 2022. Conservative
515   solute transport processes and associated transient storage mechanisms: Comparing
516   streams with contrasting channel morphologies, land use and land cover. Hydrol. Process.
517   **36**.
518 Ensign, S. H., and M. W. Doyle. 2005. In-channel transient storage and associated nutrient
519   retention: Evidence from experimental manipulations. Limnol. Oceanogr. **50**: 1740–1751.
520   doi:10.4319/lo.2005.50.6.1740
521 Ensign, S. H., and M. W. Doyle. 2006. Nutrient spiraling in streams and river networks. J.
522   Geophys. Res. Biogeosciences **111**. doi:10.1029/2005jg000114
523 Fields, J. F., and D. P. Dethier. 2019. From on high: Geochemistry of alpine springs, Niwot
524   Ridge, Colorado Front Range, USA. Hydrol. Process. **33**: 1756–1774.
525   doi:10.1002/hyp.13436
526 Francoeur, S. N., and B. J. F. Biggs. 2006. Short-term Effects of Elevated Velocity and Sediment
527   Abrasion on Benthic Algal Communities. Hydrobiologia **561**: 59–69.
528   doi:10.1007/s10750-005-1604-4
529 Gelman, A., and D. B. Rubin. 1992. Inference from Iterative Simulation Using Multiple
530   Sequences. Stat. Sci. **7**. doi:10.1214/ss/1177011136
531 Gomez, J. D., J. L. Wilson, and M. B. Cardenas. 2012. Residence time distributions in sinuosity-
532   driven hyporheic zones and their biogeochemical effects. Water Resour. Res. **48**: 1–17.
533   doi:10.1029/2012WR012180
534 González-Pinzón, R., J. Dorley, J. Singley, K. Singha, M. Gooseff, and T. Covino. 2022. TIPT:
535   The Tracer Injection Planning Tool. Environ. Model. Softw. **156**: 105504.
536   doi:10.1016/j.envsoft.2022.105504
537 González-Pinzón, R., and R. Haggerty. 2013. An efficient method to estimate processing rates in
538   streams. Water Resour. Res. **49**: 6096–6099. doi:10.1002/wrcr.20446
539 González-Pinzón, R., R. Haggerty, and A. Argerich. 2014. Quantifying spatial differences in
540   metabolism in headwater streams. Freshw. Sci. **33**: 798–811. doi:10.1086/677555
541 González-Pinzón, R., R. Haggerty, and M. Dentz. 2013. Scaling and predicting solute transport
542   processes in streams. Water Resour. Res. **49**: 4071–4088. doi:10.1002/wrcr.20280
543 González-Pinzón, R., R. Haggerty, and D. D. Myrold. 2012. Measuring aerobic respiration in
544   stream ecosystems using the resazurin-resorufin system. J. Geophys. Res. Biogeosciences
545   **117**: 1–10. doi:10.1029/2012JG001965
546 González-Pinzón, R., J. Mortensen, and D. Van Horn. 2015. Comment on "Solute-specific
547   scaling of inorganic nitrogen and phosphorus uptake in streams" by Hall et al. (2013).
548   Biogeosciences **12**: 5365–5369. doi:10.5194/bg-12-5365-2015
549 González-Pinzón, R., M. Peipoch, R. Haggerty, E. Martí, and J. H. Fleckenstein. 2016.
550   Nighttime and daytime respiration in a headwater stream. Ecohydrology **9**: 93–100.
551   doi:10.1002/eco.1615
552 Gooseff, M. N., K. E. Bencala, D. T. Scott, R. L. Runkel, and D. M. McKnight. 2005. Sensitivity
553   analysis of conservative and reactive stream transient storage models applied to field data
554   from multiple-reach experiments. Adv. Water Resour. **28**: 479–492.
555   doi:10.1016/j.advwatres.2004.11.012

556   Gooseff, M. N., D. M. McKnight, R. L. Runkel, and J. H. Duff. 2004. Denitrification and
557   hydrologic transient storage in a glacial meltwater stream, McMurdo Dry Valleys,
558   Antarctica. Limnol. Oceanogr. **49**: 1884–1895. doi:10.4319/lo.2004.49.5.1884
559   Gootman, K. S., R. G. Pinzón, J. L. A. Knapp, V. Garayburu-Caruso, and J. Cable. 2020.
560   Spatiotemporal Variability in Transport and Reactive Processes Across a First - to Fifth -
561   Order Fluvial Network Water Resources Research. 1–18. doi:10.1029/2019WR026303
562   Hall, R. J. O., E. S. Bernhardt, and G. E. Likens. 2002. Relating nutrient uptake with transient
563   storage in forested mountain streams. Limnol. Oceanogr. **47**: 255–265.
564   doi:10.4319/lo.2002.47.1.0255
565   Hall, R. O., J. L. Tank, D. J. Sobota, and others. 2009. Nitrate removal in stream ecosystems
566   measured by 15N addition experiments: Total uptake. Limnol. Oceanogr. **54**: 653–665.
567   doi:10.4319/lo.2009.54.3.0653
568   Harvey, J. W., J. K. Böhlke, M. A. Voytek, D. Scott, and C. R. Tobias. 2013. Hyporheic zone
569   denitrification: Controls on effective reaction depth and contribution to whole-stream
570   mass balance. Water Resour. Res. **49**: 6298–6316. doi:10.1002/wrcr.20492
571   Harvey, J. W., J. E. Saiers, and J. T. Newlin. 2005. Solute transport and storage mechanisms in
572   wetlands of the Everglades, south Florida. Water Resour. Res. **41**.
573   doi:10.1029/2004WR003507
574   Hill, B. H., C. M. Elonen, L. R. Seifert, A. A. May, and E. Tarquinio. 2012. Microbial enzyme
575   stoichiometry and nutrient limitation in US streams and rivers. Ecol. Indic. **18**: 540–551.
576   doi:10.1016/j.ecolind.2012.01.007
577   Jackson, T. R., S. V. Apte, R. Haggerty, and R. Budwig. 2015. Flow structure and mean
578   residence times of lateral cavities in open channel flows: influence of bed roughness and
579   shape. Environ. Fluid Mech. **15**: 1069–1100. doi:10.1007/s10652-015-9407-2
580   Jackson, T. R., R. Haggerty, S. V. Apte, A. Coleman, and K. J. Drost. 2012. Defining and
581   measuring the mean residence time of lateral surface transient storage zones in small
582   streams. Water Resour. Res. **48**. doi:10.1029/2012WR012096
583   Jackson, T. R., R. Haggerty, S. V. Apte, and B. L. O'Connor. 2013. A mean residence time
584   relationship for lateral cavities in gravel-bed rivers and streams: Incorporating streambed
585   roughness and cavity shape. Water Resour. Res. **49**: 3642–3650. doi:10.1002/wrcr.20272
586   Kasahara, T., and S. M. Wondzell. 2003. Geomorphic controls on hyporheic exchange flow in
587   mountain streams. Water Resour. Res. **39**: SBH 3-1-SBH 3-14.
588   doi:10.1029/2002wr001386
589   Katz, S. B., C. Segura, and D. R. Warren. 2018. The influence of channel bed disturbance on
590   benthic Chlorophyll a: A high resolution perspective. Geomorphology **305**: 141–153.
591   doi:10.1016/j.geomorph.2017.11.010
592   Kelleher, C., T. Wagener, B. McGlynn, A. S. Ward, M. N. Gooseff, and R. A. Payn. 2013.
593   Identifiability of transient storage model parameters along a mountain stream. Water
594   Resour. Res. **49**: 5290–5306. doi:10.1002/wrcr.20413
595   Kiel, B. A., and M. Bayani Cardenas. 2014. Lateral hyporheic exchange throughout the
596   Mississippi River network. Nat. Geosci. **7**: 413–417. doi:10.1038/ngeo2157
597   Knapp, J. L. A., R. González-Pinzón, J. D. Drummond, L. G. Larsen, O. A. Cirpka, and J. W.
598   Harvey. 2017. Tracer-based characterization of hyporheic exchange and benthic biolayers
599   in streams. Water Resour. Res. **53**: 1575–1594. doi:10.1002/2016WR019393

Knapp, J. L. A., R. González-Pinzón, and R. Haggerty. 2018. The Resazurin-Resorufin System: Insights From a Decade of "Smart" Tracer Development for Hydrologic Applications. Water Resour. Res. **54**: 6877–6889. doi:10.1029/2018WR023103

Knapp, J. L. A., and C. Kelleher. 2020. A Perspective on the Future of Transient Storage Modeling: Let's Stop Chasing Our Tails. Water Resour. Res. **56**: e2019WR026257. doi:10.1029/2019WR026257

Krause, S., J. Lewandowski, N. B. Grimm, and others. 2017. Ecohydrological interfaces as hot spots of ecosystem processes: ECOHYDROLOGICAL INTERFACES AS HOT SPOTS. Water Resour. Res. **53**: 6359–6376. doi:10.1002/2016WR019516

Lane, C. S., D. R. Lyon, and S. E. Ziegler. 2012. Cycling of two carbon substrates of contrasting lability by heterotrophic biofilms across a nutrient gradient of headwater streams. Aquat. Sci. **75**: 235–250. doi:10.1007/s00027-012-0269-0

Lautz, L. K., and D. I. Siegel. 2007. The effect of transient storage on nitrate uptake lengths in streams: an inter-site comparison. Hydrol. Process. **21**: 3533–3548. doi:10.1002/hyp.6569

Li, L., P. L. Sullivan, P. Benettin, and others. 2021. Toward catchment hydro-biogeochemical theories. Wiley Interdisc. Rev. Water **8**: 1–31. doi:10.1002/wat2.1495

Li, Z., Z. Zeng, D. Tian, and others. 2020. The stoichiometry of soil microbial biomass determines metabolic quotient of nitrogen mineralization. Environ. Res. Lett. **15**: 034005. doi:10.1088/1748-9326/ab6a26

Liu, S., T. Maavara, C. B. Brinkerhoff, and P. A. Raymond. 2022. Global Controls on DOC Reaction Versus Export in Watersheds: A Damköhler Number Analysis. Glob. Biogeochem. Cycles **36**: e2021GB007278. doi:10.1029/2021GB007278

Logue, J. B., C. A. Stedmon, A. M. Kellerman, N. J. Nielsen, A. F. Andersson, H. Laudon, E. S. Lindström, and E. S. Kritzberg. 2016. Experimental insights into the importance of aquatic bacterial community composition to the degradation of dissolved organic matter. ISME J. **10**: 533–545. doi:10.1038/ismej.2015.131

Martí, E., N. B. Grimm, and S. G. Fisher. 1997. Pre- and Post-Flood Retention Efficiency of Nitrogen in a Sonoran Desert Stream. J. North Am. Benthol. Soc. **16**: 805–819. doi:10.2307/1468173

Mulholland, P. J., and W. R. Hill. 1997. Seasonal patterns in streamwater nutrient and dissolved organic carbon concentrations: Separating catchment flow path and in-stream effects. Water Resour. Res. **33**: 1297–1306. doi:10.1029/97wr00490

Natural Resources Conservation Service. Web Soil Survey. U. S. Dep. Agric.

Navel, S., F. Mermillod-Blondin, B. Montuelle, E. Chauvet, L. Simon, and P. Marmonier. 2011. Water-Sediment Exchanges Control Microbial Processes Associated with Leaf Litter Degradation in the Hyporheic Zone: A Microcosm Study. Microb. Ecol. **61**: 968–979. doi:10.1007/s00248-010-9774-7

Niyogi, D. K., K. S. Simon, and C. R. Townsend. 2004. Land use and stream ecosystem functioning: nutrient uptake in streams that contrast in agricultural development. Arch. Für Hydrobiol. **160**: 471–486. doi:10.1127/0003-9136/2004/0160-0471

Ocampo, C., Oldham, C., and Sivapalan, M. 2020. Nitrate attenuation in agricultural catchments: Shifting balances between transport and reaction - Ocampo - 2006 - Water Resources Research - Wiley Online Library.

Oldham, C. E., D. E. Farrow, and S. Peiffer. 2013. A generalized Damköhler number for classifying material processing in hydrological systems. Hydrol. Earth Syst. Sci. **17**: 1133–1148. doi:10.5194/hess-17-1133-2013

646 Perkins, D. M., G. Yvon-Durocher, B. O. L. Demars, J. Reiss, D. E. Pichler, N. Friberg, M.
647   Trimmer, and G. Woodward. 2012. Consistent temperature dependence of respiration
648   across ecosystems contrasting in thermal history. Glob. Change Biol. **18**: 1300–1311.
649   doi:10.1111/j.1365-2486.2011.02597.x
650 Pinay, G., S. Peiffer, J.-R. De Dreuzy, and others. 2015. Upscaling Nitrogen Removal Capacity
651   from Local Hotspots to Low Stream Orders' Drainage Basins. Ecosystems **18**: 1101–
652   1120. doi:10.1007/s10021-015-9878-5
653 Ries III, K. G., J. K. Newson, M. J. Smith, and others. 2017. StreamStats, version 4.
654 Ryan, R. J., A. I. Packman, and S. S. Kilham. 2007. Relating phosphorus uptake to changes in
655   transient storage and streambed sediment characteristics in headwater tributaries of
656   Valley Creek, an urbanizing watershed. J. Hydrol. **336**: 444–457.
657   doi:10.1016/j.jhydrol.2007.01.021
658 Schmid, B. H., I. Innocenti, and U. Sanfilippo. 2010. Characterizing solute transport with
659   transient storage across a range of flow rates: The evidence of repeated tracer
660   experiments in Austrian and Italian streams. Adv. Water Resour. **33**: 1340–1346.
661   doi:10.1016/j.advwatres.2010.06.001
662 Sheibley, R. W., J. H. Duff, and A. J. Tesoriero. 2014. Low Transient Storage and Uptake
663   Efficiencies in Seven Agricultural Streams: Implications for Nutrient Demand. J.
664   Environ. Qual. **43**: 1980–1990. doi:10.2134/jeq2014.01.0034
665 Smith, R. A., R. B. Alexander, and G. E. Schwarz. 2003. Natural background concentrations of
666   nutrients in streams and rivers of the conterminous United States. Environ. Sci. Technol.
667   **37**: 3039–3047. doi:10.1021/es020663b
668 Thomas, S. A., H. Maurice Valett, J. R. Webster, and P. J. Mulholland. 2003. A regression
669   approach to estimating reactive solute uptake in advective and transient storage zones of
670   stream ecosystems. Adv. Water Resour. **26**: 965–976. doi:10.1016/S0309-
671   1708(03)00083-6
672 Tromboni, F., S. A. Thomas, B. Gücker, and others. 2018. Nutrient Limitation and the
673   Stoichiometry of Nutrient Uptake in a Tropical Rain Forest Stream. J. Geophys. Res.
674   Biogeosciences **123**: 2154–2167. doi:10.1029/2018JG004538
675 Valett, H. M., J. A. Morrice, C. N. Dahm, and M. E. Campana. 1996. Parent lithology, surface-
676   groundwater exchange, and nitrate retention in headwater streams. Limnol. Oceanogr. **41**:
677   333–345. doi:10.4319/lo.1996.41.2.0333
678 Vrugt, J. A., C. J. F. Ter Braak, C. G. H. Diks, B. A. Robinson, J. M. Hyman, and D. Higdon.
679   2009. Accelerating Markov Chain Monte Carlo Simulation by Differential Evolution
680   with Self-Adaptive Randomized Subspace Sampling. Int. J. Nonlinear Sci. Numer. Simul.
681   **10**. doi:10.1515/IJNSNS.2009.10.3.273
682 Wagner, K., M. M. Bengtsson, R. H. Findlay, T. J. Battin, and A. J. Ulseth. 2017. High light
683   intensity mediates a shift from allochthonous to autochthonous carbon use in
684   phototrophic stream biofilms. J. Geophys. Res. Biogeosciences **122**: 1806–1820.
685   doi:10.1002/2016JG003727
686 Ward, A. S., and A. I. Packman. 2019. Advancing our predictive understanding of river corridor
687   exchange. Wiley Interdiscip. Rev. Water **6**: e1327. doi:10.1002/wat2.1327
688 Ward, A. S., R. A. Payn, M. N. Gooseff, B. L. McGlynn, K. E. Bencala, C. A. Kelleher, S. M.
689   Wondzell, and T. Wagener. 2013. Variations in surface water-ground water interactions
690   along a headwater mountain stream: Comparisons between transient storage and water
691   balance analyses. Water Resour. Res. **49**: 3359–3374. doi:10.1002/wrcr.20148

692   Webster, J. R., P. J. Mulholland, J. L. Tank, and others. 2003. Factors affecting ammonium
693   uptake in streams - an inter-biome perspective. Freshw. Biol. **48**: 1329–1352.
694   doi:10.1046/j.1365-2427.2003.01094.x

695   Wen, H., and L. Li. 2018. An upscaled rate law for mineral dissolution in heterogeneous media:
696   The role of time and length scales. Geochim. Cosmochim. Acta **235**: 1–20.
697   doi:10.1016/j.gca.2018.04.024

698   Wilhelm, L., K. Besemer, L. Fragner, H. Peter, W. Weckwerth, and T. J. Battin. 2015.
699   Altitudinal patterns of diversity and functional traits of metabolically active
700   microorganisms in stream biofilms. ISME J. **9**: 2454–2464. doi:10.1038/ismej.2015.56

701   Wondzell, S. M. 2006. Effect of morphology and discharge on hyporheic exchange flows in two
702   small streams in the Cascade Mountains of Oregon, USA. Hydrol. Process. **20**: 267–287.
703   doi:10.1002/hyp.5902

704   Zarnetske, J. P., M. N. Gooseff, T. R. Brosten, J. H. Bradford, J. P. McNamara, and W. B.
705   Bowden. 2007. Transient storage as a function of geomorphology, discharge, and
706   permafrost active layer conditions in Arctic tundra streams. Water Resour. Res. **43**: 7410.
707   doi:10.1029/2005WR004816

708   Zarnetske, J. P., R. Haggerty, S. M. Wondzell, V. A. Bokil, and R. González-Pinzón. 2012.
709   Coupled transport and reaction kinetics control the nitrate source-sink function of
710   hyporheic zones. Water Resour. Res. **48**. doi:10.1029/2012wr011894

711